The Astronomical Journal, 171:171 (7pp), 2026 March https://doi.org/10.3847/1538-3881/ae38d3

Spectroscopic Characterization of WD J000801.25-350450 and Its Two Comoving Companions

Peter A. Jałowiczor[1], Thomas P. Bickle[2], J. Davy Kirkpatrick[3], Sarah L. Casewell[4], Nicola Gentile Fusillo[5,6], Adam C. Schneider[7], Jonathan Gagné[8,9], Jacqueline K. Faherty[10], Aaron M. Meisner[11], Marc J. Kuchner[12], Adam J. Burgasser[13], Austin Rothermich[10], Alexia Bravo[7], Michiharu Hyogo[1], Mark Popinchalk[10], Alex J. Brown[14], Alberto Rebassa-Mansergas[15], Raquel Murillo-Ojeda[16], and The Backyard Worlds: Planet 9 Collaboration[17]

[1] Backyard Worlds: Planet 9, USA; peter.jalowiczor@outlook.com
[2] School of Physical Sciences, The Open University, Milton Keynes, MK7 6AA, UK
[3] IPAC, Mail Code 100-22, Caltech, 1200 E. California Blvd., Pasadena, CA 91125, USA
[4] School of Physics and Astronomy, University of Leicester, Leicester, LE1 7RH, UK
[5] Department of Physics, Universitá degli Studi di Trieste, Trieste, 34127, Italy
[6] INAF-Osservatorio Astronomico di Trieste, Via G.B. Tiepolo 11, I-34143 Trieste, Italy
[7] United States Naval Observatory, Flagstaff Station, 10391, West Naval Observatory Rd., Flagstaff, AZ 86005, USA
[8] Planétarium de Montréal, Espace pour la Vie, 4801 ave. Pierre-de Coubertin, Montréal, QC H1V 3V4, Canada
[9] Trottier Institute for Research on Exoplanets, Université de Montréal, 2900 Boulevard Édouard-Montpetit Montréal, QC H3T 1J4, Canada
[10] Department of Astrophysics, American Museum of Natural History, Central Park West at 79th St., NY 10024, USA
[11] NSF National Optical-Infrared Astronomy Research Laboratory, 950 N. Cherry Ave., Tucson, AZ 85719, USA
[12] Exoplanets and Stellar Astrophysics Laboratory, NASA Goddard Space Flight Center, 8800 Greenbelt Rd., Greenbelt, MD 20771, USA
[13] Department of Astronomy & Astrophysics, UC San Diego, La Jolla, CA, USA
[14] Hamburger Sternwarte, University of Hamburg, Gojenbergsweg 112, 21029 Hamburg, Germany
[15] Departament de Física, Universitat Politècnica de Catalunya, c/Esteve Terrades 5, 08860 Castelldefels, Spain, Institute for Space Studies of Catalonia, c/Gran Capità 2–4, Edif. Nexus 104, 08034 Barcelona, Spain
[16] Centro de Astrobiología (CAB), CSIC-INTA, Camino Bajo del Castillo s/n, campus ESAC, 28692, Villanueva de la Cañada, Madrid, Spain
Received 2025 September 25; revised 2026 January 12; accepted 2026 January 13; published 2026 February 18

Abstract

We present new spectroscopic data for Gaia DR3 2309499817384726016 (WD 0008-350A) and its two wide, comoving, low-mass companions. We confirm the white dwarf is a hydrogen rich DA, with $T_{\rm eff} = 6200 \pm 90$ K and a mass of $0.63 \pm 0.03\,M_{\odot}$, close to that of the average white dwarf. Near-infrared spectra of the two stellar companions to WD 0008-350A reveal that the inner companion is an M dwarf, exhibiting a spectral type of M8. Furthermore, the outer companion is identified as a possible M6 + M9 binary. This paper examines the evidence which suggests the system may be quadruple.

Unified Astronomy Thesaurus concepts: M dwarf stars (982); DA stars (348); Multiple stars (1081)

1. Introduction

A significant proportion of the stars in the Milky Way are found in multiple systems. The reasons for the different hierarchies are crucial to understanding the stellar formation process, and multiple systems containing white dwarfs are important to understand how these systems evolve. White dwarfs in multiple stellar systems are essential for investigating how stellar interactions with companion stars influence stellar evolution (F. Lagos et al. 2022). Studying hierarchical systems helps refine stellar evolution models in multiple systems. This includes processes such as the evolution of white dwarf binaries during any mass-transfer phase (N. Ivanova & R. E. Taam 2004), tidal interactions, and common-envelope phases (I. Iben & M. Livio 1993) as well as the initial formation of the system (B. D. Mason et al. 2018).

Backyard Worlds: Planet 9 (BYW: P9; M. J. Kuchner et al. 2017) uses citizen science to search images from the *Wide-field Infrared Survey Explorer* mission (WISE; E. L. Wright et al. 2010) for moving objects: brown dwarfs and stars with high proper motions, and new planets in the outer solar system (e.g., K. Batygin & M. E. Brown 2016). The project identified 112 objects in the 20 pc full-sky census of J. D. Kirkpatrick et al. (2024). Since its inception, the BYW:P9 project has expanded its scope, resulting in the Backyard Worlds: Cool Neighbours project. This uses machine learning to discover Y dwarf candidates. BYW: P9 has also seen success with the discovery of exotic objects such as extreme T-type subdwarfs (A. C. Schneider et al. 2020; A. M. Meisner et al. 2021), low-mass companions to other stars (J. K. Faherty et al. 2021; A. Rothermich et al. 2024), and previous discoveries in the white dwarf field (J. H. Debes et al. 2019; P. A. Jalowiczor et al. 2021; T. P. Bickle et al. 2022).

In this paper, we discuss Gaia DR3 2309499817384726016 or WDJ000801.25-350450.2 (WD 0008-350A), comprised of a WD primary, in a higher-order hierarchy with two (or three) low-mass stellar companions. We independently identified this system as part of the BYW: P9 science project, hosted on the Zooniverse platform. We have characterized this newly discovered system with spectroscopy of each component. The system is described in Section 2. The observations of the system are described in Section 3, and the analysis of the new data is described in Section 4. The system, in the context of other known WD multiples, is discussed in Section 5.

[17] backyardworlds.org

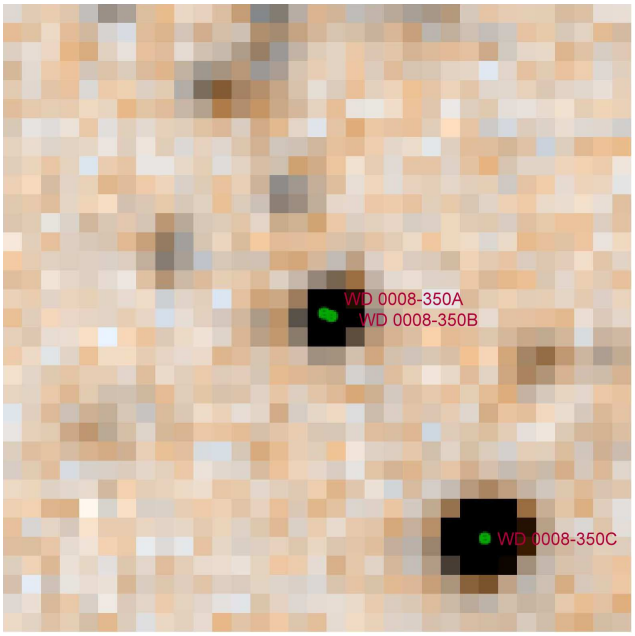

Figure 1. The "Family Portrait," a pseudo-color composite image of this system. This was created from WISE instrument bands. Blue represents the W1 band. Red represents the W2 band. Green represents the average of the W1 and W2 bands. The green dots are the Gaia Overlay; they indicate that a celestial object has already been cataloged in the Gaia database. The field of view is $90'' \times 90''$.

2. The WDJ000801.25-350450.2 System

Figure 1 was constructed using the `WiseView` tool (D. Caselden et al. 2018) from data acquired by the WISE mission. The image is a composite of unWISE coadds (A. M. Meisner et al. 2018) from two specific mid-infrared filter bands. These are the WISE W1 (centered at 3.4 (μm)) and W2 bands (centered at 4.6 (μm)). This combination helps visualize objects with different infrared properties, since the W1 and W2 bands are centered on different infrared wavelengths.

N. P. Gentile Fusillo et al. (2021) first identified WD 0008-350A with a probability of being a white dwarf of 0.78, $T_{\rm eff} = 4673 \pm 180$ K and $\log g = 6.975 \pm 0.233$ and a mass of $0.18 \pm 0.06\ M_{\odot}$. O. Vincent et al. (2024) subsequently used the Gaia XP spectra to determine that WD 0008-350A is a Hydrogen-rich DA white dwarf with $T_{\rm eff} = 5378 \pm 108$ K and $\log g = 7.396 \pm 0.063$ with a mass of $0.292 \pm 0.033\ M_{\odot}$. The masses determined by both N. P. Gentile Fusillo et al. (2021) and O. Vincent et al. (2024) are very low for a white dwarf, well below the average of $\sim 0.6\ M_{\odot}$ (S. O. Kepler et al. 2017). The presence of the close companion Gaia DR3 2309499813089120512 at $1\farcs1$ away presents a potential source of photometric contamination that could have influenced the Gaia photometry. The G_{BP} magnitude is faint, and the contaminating target is an M dwarf, making the total flux appear brighter at longer wavelengths, suggesting a cooler, but physically larger white dwarf.

WDJ000801.25-350450.2 was also identified as part of a multiple system by A. Tokovinin (2022), who listed it in their Gaia triple system compilation. They list the white dwarf as component B, although they do not acknowledge it as a white dwarf, and present two suggested companions, Gaia DR3 2309499813089120512 (C) and Gaia DR3 2309499778729380480 (A), separated from the primary by $1\farcs1$ and $39\farcs48$, respectively. They determined the masses of the three components to be 0.13, 0.10 and 0.14 $M_{\odot}$ from their absolute magnitudes, assuming all components are on the main sequence.

P. Kervella et al. (2022) also identified this system using proper motion anomaly as a primary selection criterion for targeted direct imaging campaigns. Candidates exhibiting a significant proper motion anomaly were identified as promising candidates for hosting a companion. They determined the respective masses in this system to be 0.11, 0.11 and 0.14 $M_{\odot}$.

3. Observations

3.1. Very Large Telescope (VLT)/X-Shooter

WD 0008-350A was observed on UT 2024 September 2 with the X-Shooter spectrograph (J. Vernet et al. 2011) mounted on UT2 of ESO's VLT located in Paranal, Chile, as part of program 113.26HT.001 (PI: Casewell). We obtained spectra in the UVB (0.30−0.56 m) and VIS (0.56−1.01 μm) arms using slit widths of $1''$ and $0\farcs9$, respectively, on the night of 2024 September 2 and using an exposure time of 660 s in stare mode. We reduced the data using the standard `ESOREFLEX` pipeline to perform flat-fielding, bias correction, and apply the wavelength correction.

3.2. Infrared Telescope Facility (IRTF)/SpeX

WD 0008-350B and WD 0008-350C were observed on UT 2024 August 13 using the SpeX spectrograph (J. T. Rayner et al. 2003) on NASA's IRTF telescope. SpeX was operated in prism mode using the $0\farcs8 \times 15''$ slit, providing an average resolution of $\sim$200 over the 0.8−2.5 μm wavelength range. The objects were observed using an AB nod pattern along the slit. For the inner companion, we obtained eight 150 s exposures, and for the outer companion, we obtained eight 90 s exposures. Due to their proximity on the sky, the two companions were observed consecutively, at an average airmass of 1.76. For telluric correction, the A0 star HD 225200 was observed immediately after the targets, followed by internal flat-field and arc lamp exposures for calibration. Data were reduced using the `Spextool` package (M. C. Cushing et al. 2004) with telluric correction and flux calibration of the A0 star performed using procedures described in W. D. Vacca et al. (2003).

4. Analysis

4.1. WD 0008-350, Primary

To obtain a set of spectroscopic stellar parameters for the white dwarf, we fit the continuum-normalized Balmer line profiles in the X-Shooter UVB and VIS spectra with the grid of 3D pure-hydrogen (DA, e.g., hydrogen dominated) local thermal equilibrium atmosphere models described in P. E. Tremblay et al. (2013) and P. E. Tremblay et al. (2015). A complete description of models' input physics is available on P.-E. Tremblay's Source Model Data webpage.[18]

From our best-fitting model, we determine $T_{\rm eff} = 6200 \pm 90$ K and $\log g = 8.08 \pm 0.6$. These values are presented in Table 1. Figure 2 shows the spectral fitting to the white dwarf (red overlay), noting that the white dwarf's spectrum is

[18] https://warwick.ac.uk/fac/sci/physics/research/astro/people/tremblay/modelgrids/

Table 1
System Properties

Parameter	WD 0008-350A	WD 0008-350B	WD 0008-350C	References
Mass ($M_\odot$)	0.63 ± 0.03	0.08	0.10	(0)
R.A. (degrees)	2.0057513	2.0054037	1.997907	(1)
decl. (degrees)	−35.080540	−35.0806593	−35.0895739	(1)
$T_{\rm eff}$	6200 ± 90 K	⋯	⋯	(2)
$T_{\rm eff}$	⋯	2572 ± 190 K	2660 ± 184 K	(3)
log g	8.08 ± 0.6	⋯	⋯	(0)
RUWE	1.000	1.029	1.205	(1)
ϖ (mas)	11.00 ± 0.20	11.10 ± 0.6	10.80 ± 0.2	(1)
μ_α (mas yr^{-1})	92.92 ± 0.14	90.7 ± 0.4	91.55 ± 0.17	(1)
μ_δ (mas yr^{-1})	-19.61 ± 0.63	-15.7 ± 0.8	-17.80 ± 0.23	(1)
G (mag)	18.73 ± 0.003	20.21 ± 0.008	18.32 ± 0.004	(1)
$G_{\rm Bp}$ (mag)	19.02 ± 0.030	⋯	20.73 ± 0.123	(1)
$G_{\rm Rp}$ (mag)	17.83 ± 0.026	⋯	16.82 ± 0.009	(1)
J(mag)	⋯	15.76 ± 0.07	14.42 ± 0.03	(4)
H(mag)	⋯	15.02 ± 0.10	13.75 ± 0.02	(4)
K(mag)	⋯	14.62 ± 0.10	13.39 ± 0.03	(4)
$W1$(mag)	⋯	14.30 ± 0.03	13.16 ± 0.02	(5)
$W2$(mag)	⋯	14.10 ± 0.04	12.93 ± 0.03	(5)

References. (0) This work, (1) Gaia DR3 (Gaia Collaboration et al. 2023), (2) P. E. Tremblay et al. (2013), (3) A. Sanghi et al. (2023), (4) M. Skrutskie et al. (2007), (5) E. L. Wright et al. (2010).

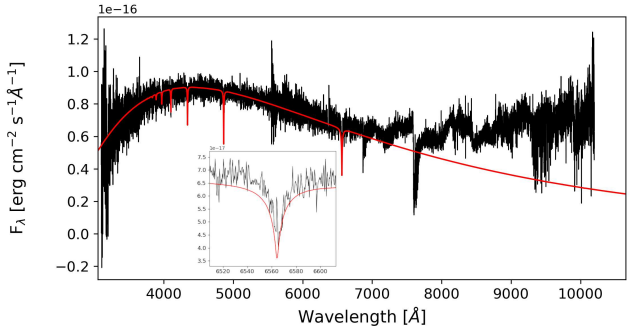

Figure 2. X-Shooter spectrum of WD 0008-350A. The best-fit model to the white dwarf is shown in red overlay. The spectrum is blended with WD 0008-350B, evidenced by the flux excess past ∼7000 Å. The sub-figure provides a magnified view of the Hα line.

partially blended with that of the inner companion (B) beyond about 7500 Å.

Although the effective temperature is broadly consistent with the previous determinations of N. P. Gentile Fusillo et al. (2021) and O. Vincent et al. (2024), the gravity determination has increased significantly with the X-Shooter spectra. This is likely due to the much higher signal-to-noise ratio of the spectrum as well as the broader wavelength coverage than that provided by Gaia. However, XP spectra offer a more enhanced spectral classification along with more precise determinations of the effective temperature and surface gravity.

We used `wdwarfdate` (R. Kiman et al. 2022) which, when provided with effective temperature, surface gravity and their respective uncertainties, uses the MIST isochrones (J. Choi et al. 2016; A. Dotter 2016), the J. D. Cummings et al. (2019) initial–final mass relation and the A. Bédard et al. (2020) cooling models to estimate the cooling age, total age, initial main-sequence mass and the current mass of a white dwarf. Using the DA model, which incorporates the DA mass–radius (M–R) relation with thick hydrogen layers and carbon oxygen cores of A. Bédard et al. (2020),[19] we determine a total age for WDJ0008-350 of $4.67^{+3.58}_{-0.85}$ Gyr, with a cooling age of $2.45^{+0.24}_{-0.39}$ Gyr. We estimate a progenitor mass of $1.65^{+0.56}_{-0.44}\,M_\odot$ and a current mass of $0.63 \pm 0.03\ M_\odot$. For the purposes of this analysis, we assume solar metallicity and $v/v_{\rm crit} = 0$, where v/v_{crit} represents the object's velocity as a fraction of its critical (or break-up) velocity.

The absence of a detectable H-beta (Hβ) emission feature in the spectrum (Figure 2) strongly suggests that the apparent feature at the H-alpha (Hα) wavelength is not a true emission line.

In Table 1, the RUWE for WD 0008-350A = 1.000. This indicates the observed star's motion is well-modeled by the single-star solution (L. Lindegren et al. 2021).

4.2. WD 0008-350B, Inner Companion

To determine the spectral type of the inner companion, Gaia 2309499813089120512 (WD 0008-350B), its SpeX spectrum was compared to M dwarf near-infrared spectral standards from J. D. Kirkpatrick et al. (2010). All spectra were normalized between 1.27 and 1.29 μm and visually compared to determine the best overall fit. The best fit was determined to be the M8 standard (VB 10), which is plotted against the spectrum of the WD 0008-350B in Figure 3. The fit is excellent over the 0.9−2.4 μm range, though WD 0008-350B displays some flux excess at wavelengths $< 0.9\mu$m, potentially due to contamination from the white dwarf.

We derived the effective temperature ($T_{\rm eff}$) using empirical relationships for bolometric luminosity ($L_{\rm bol}$) and $T_{\rm eff}$ as presented in A. Sanghi et al. (2023). This gives an effective temperature of 2572 ± 190 K for the inner companion.

M. J. Pecaut & E. E. Mamajek (2013) presents a collection of empirical relationships and tables that link the effective temperature $T_{\rm eff}$ to the star's spectral type and color. The stellar mass is subsequently determined by positioning the star

[19] https://www.astro.umontreal.ca/~bergeron/CoolingModels/

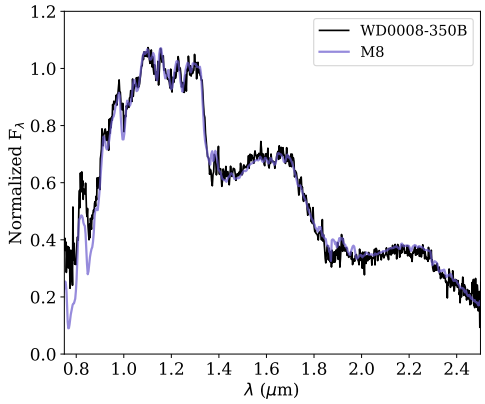

Figure 3. IRTF/SpeX spectrum of the inner companion (black) compared to the M8 spectral standard, VB 10 (blue) from J. D. Kirkpatrick et al. (2010). All spectra are normalized between 1.27 and 1.29 μm

on a Hertzsprung–Russell (H-R) diagram and comparing its location, as indicated by its luminosity and temperature, to theoretical evolutionary tracks from stellar models.

Utilizing stellar evolutionary tracks in M. J. Pecaut & E. E. Mamajek (2013), our analysis resulted in a mass of 0.08 $M_\odot$ for WD 0008-350B. This value was obtained by identifying where the star's effective temperature ($T_{\rm eff}$) intersected with the appropriate evolutionary track on a model H-R diagram.

In Table 1, the RUWE for WD 0008–350B is 1.029; this also indicates a good fit to the single-star solution (L. Lindegren et al. 2021).

4.3. WD 0008-350C, Outer Companion

The outer companion was identified by C. Reylé (2018) as an ultracool dwarf candidate based on its position on Gaia DR2 (Gaia Collaboration et al. 2018) and 2MASS (M. F. Skrutskie et al. 2006) color–magnitude and color–color diagrams. They determined a photometric spectral type of M7.

We compared the SpeX spectrum of Gaia DR3 2309499778729380480 (WD 0008-350C) to near-infrared M and L dwarf spectral standards from J. D. Kirkpatrick et al. (2010). The single best-fitting standard for the C component was the M6 standard LHS 1375.

For a single template, the M6 standard exhibited an overall agreement with a χ^2 of 30, with the M5 and M7 standards giving χ^2 values of 126 and 43, respectively. We also assessed binary template configurations to attain the highest degree of agreement with the empirical spectra using the methods in A. Bravo et al. (2025).

We applied near-infrared M dwarf standards from J. D. Kirkpatrick et al. (2010), combined with 2MASS near-infrared photometry and Gaia DR3 parallax measurements, to create template binary spectra. The best-fitting binary template was M6 + M9, where the M9 standard is LHS 2924. The M6 + M9 solution is a significantly better fit ($\chi^2_\nu = 9.3$) than the single-spectrum M6 solution ($\chi^2_\nu = 30.1$). Consequently, the high value of $\chi^2_\nu = 30.1$ demonstrates that the single-spectrum M6 solution is statistically improbable and should be rejected in favor of a more robust model. The binary spectral templates resulted in a significantly lower χ^2_ν value, which indicates a more robust and physically plausible fit. For both the single and binary fits, we exclude wavelength regions between 1.35 and 1.45 μm as well as between 1.81 and 1.95 μm because these regions can be heavily impacted by telluric absorption.

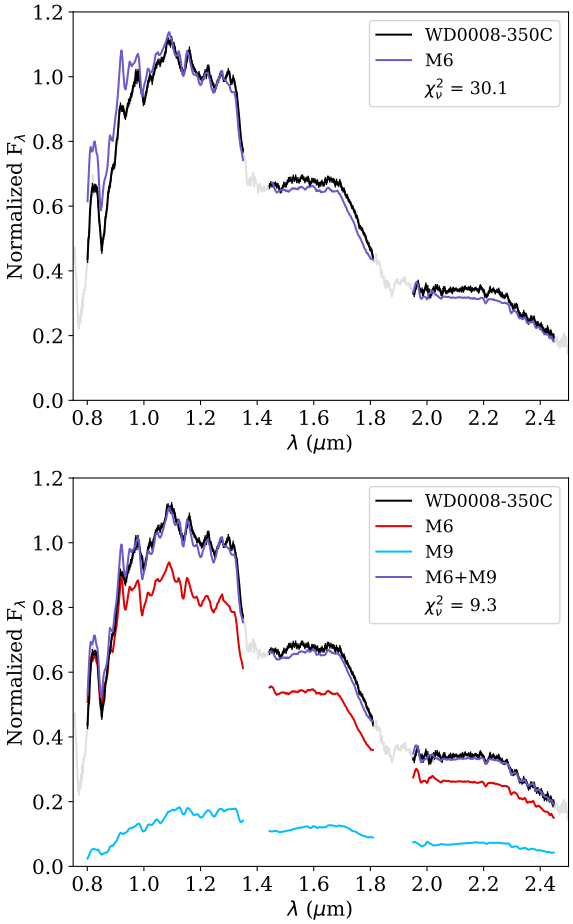

Figure 4. Single and binary template fits for the C component. The full spectrum of WD 0008-350C is shown in gray, while the regions used for the template fits are shown in black. The single fit (top) uses the M6 standard LHS 1375. The binary fit (bottom) for the C component M6+M9 uses the M9 standard LHS 2924.

Figure 4 shows the results of fitting binary templates to the C component, where it can be seen that the shorter wavelength part of the spectra is a much better fit by the binary template. We note an important caveat that the observed discrepancy is entirely attributable to the M6 template being excessively blue. Although the M6 template indeed appears too blue in certain spectral regions, it is too red at shorter wavelengths ($\lambda < 0.9$ μm). This indicates that a simple instrumental effect is an unlikely sole explanation, unless such an effect can differentially impact distinct portions of the spectrum in different ways.

Using the spectral type versus mass/radius trends presented in Table 5 of M. J. Pecaut & E. E. Mamajek (2013), we estimate the mass of WD 0008-350C to be 0.10 $M_\odot$, consistent with an M6 spectral type. However, if we adopt the mass of the outer companion as M6 + M9 then we determine a value of 0.18 $M_\odot$.

We detected no variability in the TESS light curve of WD 0008-350C that could be due to a reflection effect or variability. This is likely due to the object's faintness, with a Gaia G-band magnitude of 18.32 which is below the effective photometric precision limit of the TESS-Gaia Light Curve (TGLC) dataset.

In Table 1, the RUWE for WD 0008-350C is 1.205; a threshold of RUWE $\leqslant$ 1.4 indicates a well-behaved solution (L. Lindegren et al. 2021). The Gaia IPD parameter (the fraction of multipeak image parameter determination) transits is 0. These parameters also constrain any object that is unresolved in the Gaia astrometric data. It is consistent with the reported absence of any companions beyond an angular separation of 0.″3. Although the template fitting procedure favors a binary solution, constraints imposed by the Gaia data limit the range of possible binary configurations. Specifically, the RUWE and IDP values from Gaia effectively rule out many potential orbital solutions. Therefore, additional high-resolution observations are necessary to confirm or refute the inferred binary nature of this source.

We also investigated the near-infrared colors of the *C* component of this system to see whether or not they might provide additional evidence of its multiplicity. We find $J - H$ and $H - K$ colors of 0.67 ± 0.04 mag and 0.36 ± 0.04 mag, respectively compared to the median $J - H$ ($0.60^{+0.06}_{-0.05}$ mag) and $H - K$ (0.33 ± 0.05 mag) colors of $M6 - M6.9$ dwarfs from W. M. J. Best et al. (2018), the values for WD 0008-350C are redder, but within $\sim 1\sigma$ of the median values in both cases. While these redder generally support the binary hypothesis for this component of this system, additional observations are likely needed to determine its potential multiplicity definitively.

5. System Properties

5.1. Comoving Probability

Initially, we utilized the `WiseView` tool (D. Caselden et al. 2018) to look for any additional companions which were not detected by Gaia (e.g., brown dwarfs). `WiseView` blinks time-resolved WISE W1 & W2 coadds spanning ~12 yrs to create a time-lapse video for a specified region of sky, allowing for convenient visualization of proper motion. It also contains a Gaia DR3 overlay, which displays the Gaia proper motion, which allowed for easy visual comparison. Using this technique, we have ruled-out any additional low-mass companions in the system out to a separation of approximately 100″.

Faint companions are hard to distinguish from much brighter primaries in WISE because of the low angular resolution.

`CoMover` (J. Gagné et al. 2021) was employed to determine the probability that the host white dwarf and the stellar companions are comoving and therefore likely to be gravitationally bound. `CoMover` uses a framework similar to the BANYAN Σ Bayesian classification algorithm. The comoving probability is determined by comparing a model of the potential companion's motion against models of both the field stars and the host star.

The main difference between BANYAN Σ and `CoMover` is that `CoMover` only includes models of field stars (see J. Gagné et al. 2018 for more detail). The `CoMover` algorithm marginalizes over any missing parameters (such as the radial velocity or parallax of the companion) to compute the probability density in *XYZUVW* space directly, using the analytical solutions to the marginalization integrals provided in J. Gagné et al. (2018). The resulting probability densities are compared using Bayes' theorem to determine the co-moving probability.

For this system, both the inner and outer pairs exhibit a co-moving probability exceeding 99.9%. The log probability of the field hypothesis is −11.8 for the outer companion-primary pair. This corresponds to an extremely small probability of non-association: 7.45×10^{-6} for the outer pair. A potential limitation is that the calculated comoving probabilities are model-dependent. This introduces a caveat: inaccuracies in the models of either the host star or nearby field stars could lead to an overestimation of the comoving probability.

5.2. Orbital Characteristics

We applied Kepler's laws to determine the orbital characteristics of the components within the triple system WD 0008-350ABC. Assuming circular orbits, and incorporating our stellar masses of $0.63 \pm 0.03\ M_\odot$ for WD 0008-350A, $0.08\ M_\odot$ for WD 0008-350B, and $0.10\ M_\odot$ for WD 0008-350C (M6, single) and $0.18\ M_\odot$ (M6 + M9 binary). Using parallax and co-ordinates from the Gaia mission, the companions were found to be ~100 au and ~3,600 au from the primary, WD 0008-350 A.

The inner companion (WD 0008-350B) was found to have an orbital period of ~1200 yr, while the outer companion (WD 0008-350C) has a period of ~240,000 yr. We utilized the mass of the outer companion, as determined by the M6 fit, to calculate the system's periods. Although the M6 + M9 template is a superior overall fit to the spectrum, the singular M6 model was adopted here pending future confirmation whether the outer companion is single or binary in nature.

Gaia satellite measurements of the relative motion between components in a hierarchical system can be used to validate or constrain orbital estimates.

The kinematic data in Table 1 show the proper motion of Component C to be consistent with the average proper motion of Components A and B. This suggests the motion of Component C represents the true systemic proper motion (μ_{sys}) of the system.

This supports the hypothesis that the measured offsets between Components A and B are attributable to orbital motion within the system. The measured PM difference between A and B is 5.8 mas yr^{-1}. It is comparable to the estimated relative motion of 4.5 mas yr^{-1} in a circular face-on orbit. The Gaia data alone are not sufficient to define the inclination and eccentricity of the AB orbit.

The current astrometric precision is insufficient to rule out a face-on circular orbit configuration. Distinguishing this specific orbital geometry from the systemic motion would necessitate an increase in precision to approximately 0.01 mas yr^{-1}.

5.3. Long-term Stability

In a sample of 392 low-mass hierarchical triple stellar systems within 100 pc resolved by Gaia, the median projected separations of the inner and outer pairs were 151 and 2569 au, respectively (A. Tokovinin 2022). The system exhibits an "average" separation, characterized by inner and outer pair distances of approximately ~100 au and ~3,600 au, respectively.

For a hierarchical triple system with an inner separation of a_{in} and an outer separation of a_{out} - the point at which stability breaks down generally depends on the separation ratio $\alpha \equiv a_{in}/a_{out}$ (M. Tory et al. 2022). $\alpha \approx 1$ suggests a highly chaotic system. For this system, $\alpha = 0.028$. This system is therefore very stable, far from the threshold of instability.

6. Conclusion

New spectroscopic data have been presented for all components of this system. Subsequently, the WD mass is revised from $M = 0.18 \pm 0.06\ M_{\odot}$ to $M = 0.63 \pm 0.04\ M_{\odot}$. Our analysis yielded mass estimates of 0.08 $M_{\odot}$ and 0.10 $M_{\odot}$ (M6, single) or 0.18 $M_{\odot}$ (M6 + M9, binary) for the two outermost companions.

Our spectrally inferred masses are, respectively, slightly lower for the outer two companions when compared with the photometrically derived masses of 0.13 $M_{\odot}$ and 0.14 $M_{\odot}$ A. Tokovinin (2022) and 0.11 $M_{\odot}$ and 0.14 $M_{\odot}$ P. Kervella et al. (2022).

We determine the following: a total age of $4.67^{+3.58}_{-0.85}$ Gyr for the system; a main-sequence age of $2.15^{+3.83}_{-1.04}$ Gyr for the progenitor; an initial stellar mass of the WD 0008-350A estimated at $1.65^{+0.56}_{-0.44}\ M_{\odot}$.

The inner companion's spectral class is determined to be M8. A spectral binary template of M6+M9 best matches the outer companion's spectral type. The template fitting procedure favors a binary stellar configuration. However, the range of viable binary solutions is significantly constrained by the Gaia data. Further analysis, such as high-resolution imaging or radial velocity monitoring, may confirm the binary or single nature of this object. The TESS light curve of WD 0008-350C showed no detectable photometric variability.

This stellar configuration represents a relatively rare hierarchical system, comprising either three or four components. Such systems are invaluable for estimating the age of their ultracool stellar companions, as their ages can be directly linked to the more accurately determined age of the white dwarf primary. Should this system be definitively confirmed as a WD + 3 hierarchical configuration, its occurrence rate would fall below the 1.9% for quadruple systems as reported by P. P. Eggleton & A. A. Tokovinin (2008). This highlights its unique nature and importance for refining our understanding of multiple-stellar system demographics.

With $\alpha = 0.029$, this system represents a stable configuration.

Additional observational data beyond those provided by Gaia are required to constrain the orbital inclinations and eccentricities in this system.

The current astrometric precision is insufficient to exclude a face-on circular orbit configuration.

Acknowledgments

The Backyard Worlds: Planet 9 team would like to thank the many Zooniverse volunteers who have participated in this project. We would also like to thank the Zooniverse web development team for their work creating and maintaining the Zooniverse platform and the Project Builder tools. This research was supported by NASA grant 2017-ADAP17-0067. This material is supported by the National Science Foundation under grant Nos. 2007068, 2009136, and 2009177. Based on observations collected at the European Organisation for Astronomical Research in the Southern Hemisphere under ESO program(s) 113.26HT.001. Data were also taken by Visiting Astronomers at the Infrared Telescope Facility, which is operated by the University of Hawaii under contract 80HQTR24DA010 with the National Aeronautics and Space Administration. This work has made use of data from the European Space Agency (ESA) mission Gaia (https://www.cosmos.esa.int/gaia), processed by the Gaia Data Processing and Analysis Consortium (DPAC; https://www.cosmos.esa.int/web/gaia/dpac/consortium). Funding for the DPAC has been provided by national institutions, in particular the institutions participating in the Gaia Multilateral Agreement, This publication makes use of data products from the *Wide-field Infrared Survey Explorer* (WISE), which is a joint project of the University of California, Los Angeles, and the Jet Propulsion Laboratory/ California Institute of Technology, funded by the National Aeronautics and Space Administration. RMO is funded by INTA through grant PRE-OBSERVATORIO and acknowledges support from project PID2023-146210NB-I00 funded by MICIU/AEI/10.13039/501100011033 and by ERDF/EU.

Software: CalcTool (https://www.calctool.org/astrophysics); CoMover (J. Gagné et al. 2021); Lightkurve (Lightkurve Collaboration et al. 2018) WiseView (D. Caselden et al. 2018); WDWARFDATE (R. Kiman et al. 2022).

ORCID iDs

Peter A. Jałowiczor https://orcid.org/0000-0002-4175-295X
Thomas P. Bickle https://orcid.org/0000-0003-2235-761X
J. Davy Kirkpatrick https://orcid.org/0000-0003-4269-260X
Sarah L. Casewell https://orcid.org/0000-0003-2478-0120
Nicola Gentile Fusillo https://orcid.org/0000-0002-6428-4378
Adam C. Schneider https://orcid.org/0000-0002-6294-5937
Jonathan Gagné https://orcid.org/0000-0002-2592-9612
Jacqueline K. Faherty https://orcid.org/0000-0001-6251-0573
Aaron M. Meisner https://orcid.org/0000-0002-1125-7384
Marc J. Kuchner https://orcid.org/0000-0002-2387-5489
Adam J. Burgasser https://orcid.org/0000-0002-6523-9536
Austin Rothermich https://orcid.org/0000-0003-4083-9962
Alexia Bravo https://orcid.org/0009-0002-3936-8059
Michiharu Hyogo https://orcid.org/0000-0001-8343-0820
Mark Popinchalk https://orcid.org/0000-0001-9482-7794
Alex J. Brown https://orcid.org/0000-0002-3316-7240
Alberto Rebassa-Mansergas https://orcid.org/0000-0002-6153-7173
Raquel Murillo-Ojeda https://orcid.org/0009-0002-8578-0765

References

Batygin, K., & Brown, M. E. 2016, AJ, 151, 22
Bédard, A., Bergeron, P., Brassard, P., & Fontaine, G. 2020, ApJ, 901, 93
Best, W. M. J., Magnier, E. A., Liu, M. C., et al. 2018, ApJS, 234, 1
Bickle, T. P., Jalowiczor, P. A., Casewell, S. L., et al. 2022, RNAAS, 6, 127
Bravo, A., Schneider, A. C., Casewell, S., et al. 2025, AJ, 169, 100
Caselden, D., Westin, P.I., Meisner, A., Kuchner, M., & Colin, G. 2018, WiseView: Visualizing motion and variability of faint WISE sources, Astrophysics Source Code Library, ascl:1806.004
Choi, J., Dotter, A., Conroy, C., et al. 2016, ApJ, 823, 102
Cummings, J. D., Kalirai, J. S., Choi, J., et al. 2019, ApJL, 871, L18
Cushing, M. C., Vacca, W. D., & Rayner, J. T. 2004, PASP, 116, 362
Debes, J. H., Thévenot, M., Kuchner, M. J., et al. 2019, ApJL, 872, L25
Dotter, A. 2016, ApJS, 222, 8
Eggleton, P. P., & Tokovinin, A. A. 2008, MNRAS, 389, 869
Faherty, J. K., Gagné, J., Popinchalk, M., et al. 2021, ApJ, 923, 48
Gagné, J., Faherty, J. K., Schneider, A. C., & Meisner, A. M. 2021, CoMover: Bayesian probability of co-moving stars, Astrophysics Source Code Library, ascl:2106.007
Gagné, J., Mamajek, E. E., Malo, L., et al. 2018, ApJ, 856, 23
Gaia Collaboration, Brown, A. G. A., Vallenari, A., et al. 2018, A&A, 616, A1
Gaia Collaboration, Vallenari, A., Brown, A. G. A., et al. 2023, A&A, 674, A1
Gentile Fusillo, N. P., Tremblay, P. E., Cukanovaite, E., et al. 2021, MNRAS, 508, 3877
Iben, I., & Livio, M. 1993, PASP, 105, 1373
Ivanova, N., & Taam, R. E. 2004, ApJ, 601, 1058

Jalowiczor, P. A., Casewell, S., Schneider, A. C., et al. 2021, RNAAS, 5, 76
Kepler, S. O., Koester, D., Romero, A. D., Ourique, G., & Pelisoli, I. 2017, in 20th European White Dwarf Workshop, ed. P.-E. Tremblay et al. (ASP), 421
Kervella, P., Arenou, F., & Thévenin, F. 2022, A&A, 657, A7
Kiman, R., Xu, S., Faherty, J. K., et al. 2022, AJ, 164, 62
Kirkpatrick, J. D., Looper, D. L., Burgasser, A. J., et al. 2010, ApJS, 190, 100
Kirkpatrick, J. D., Marocco, F., Gelino, C. R., et al. 2024, ApJS, 271, 55
Kuchner, M. J., Faherty, J. K., Schneider, A. C., et al. 2017, ApJL, 841, L19
Lagos, F., Zorotovic, M., Schreiber, M. R., & Gänsicke, B. T. 2022, MNRAS, 519, 2302
Lightkurve Collaboration, Cardoso, J. V. d. M., Hedges, C., et al. 2018, Lightkurve: Kepler and TESS time series analysis in Python, Astrophysics Source Code Library, ascl:1812.013
Lindegren, L., Klioner, S. A., Hernández, J., et al. 2021, A&A, 649, A2
Mason, B. D., Hartkopf, W. I., Miles, K. N., et al. 2018, AJ, 155, 215
Meisner, A. M., Lang, D., & Schlegel, D. J. 2018, AJ, 156, 69
Meisner, A. M., Schneider, A. C., Burgasser, A. J., et al. 2021, ApJ, 915, 120
Pecaut, M. J., & Mamajek, E. E. 2013, ApJS, 208, 9
Rayner, J. T., Toomey, D. W., Onaka, P. M., et al. 2003, PASP, 115, 362
Reylé, C. 2018, A&A, 619, L8
Rothermich, A., Faherty, J. K., Bardalez-Gagliuffi, D., et al. 2024, AJ, 167, 253
Sanghi, A., Liu, M. C., Best, W. M., et al. 2023, ApJ, 959, 63
Schneider, A. C., Burgasser, A. J., Gerasimov, R., et al. 2020, ApJ, 898, 77
Skrutskie, M., Cutri, R., Stiening, R., et al. 2007, AJ, 131, 1163
Skrutskie, M. F., Cutri, R. M., Stiening, R., et al. 2006, AJ, 131, 1163
Tokovinin, A. 2022, ApJ, 926, 1
Tory, M., Grishin, E., & Mandel, I. 2022, PASA, 39, e062
Tremblay, P. E., Gianninas, A., Kilic, M., et al. 2015, ApJ, 809, 148
Tremblay, P. E., Ludwig, H. G., Steffen, M., & Freytag, B. 2013, A&A, 559, A104
Vacca, W. D., Cushing, M. C., & Rayner, J. T. 2003, PASP, 115, 389
Vernet, J., Dekker, H., D'Odorico, S., et al. 2011, A&A, 536, A105
Vincent, O., Barstow, M. A., Jordan, S., et al. 2024, A&A, 682, A5
Wright, E. L., Eisenhardt, P. R. M., Mainzer, A. K., et al. 2010, AJ, 140, 1868